

The actual impedance of non-reflecting  
boundary conditions: implications for the  
computation of resonators

**Laurent Selle**, \*  
CERFACS Toulouse  
**Franck Nicoud** †  
University Montpellier II  
and  
**Thierry Poinsot** ‡  
IMF Toulouse, UMR5502, Toulouse

June 20, 2003

---

\*Corresponding author: CERFACS, 42 avenue G. Coriolis, 31057 Toulouse, France.  
e-mail: selle@cerfacs.fr

†University Montpellier II, Math Dept. - ACSIOM Lab. - CC51, 34095 Montpellier  
Cedex 5, France.

‡Member AIAA. IMFT Allee du Professeur Camille SOULA 31400 Toulouse, France

## Abstract

Non-reflecting boundary conditions are essential elements in the computation of many compressible flows: such simulations are very sensitive to the treatment of acoustic waves at boundaries. Non-reflecting conditions allow acoustic waves to propagate through boundaries with zero or small levels of reflection into the domain. Perfectly non-reflecting conditions must however be avoided because they can lead to an ill-posed problem for the mean flow. Various methods have been proposed to construct boundary conditions which can be sufficiently non-reflecting for the acoustic field while still making the mean flow problem well-posed. This paper analyses a widely used technique for non-reflecting outlets (Rudy and Strikwerda, Poinsot and Lele): it is shown that the correction introduced by these authors can lead to large reflection levels and non-physical resonant behaviours. A simple scaling is proposed to evaluate the relaxation coefficient used in these methods for a non-reflecting outlet. The proposed scaling is tested for simple cases (ducts) both theoretically and numerically.

# 1 Introduction

Deriving non-reflecting boundary conditions for hyperbolic or incompletely hyperbolic problems<sup>1</sup> is a key problem in multiple fields such as classical engineering fluid dynamics<sup>2,3,4,5,6,7,8</sup>, aeroacoustics<sup>9,10,11,12</sup>, astrophysics<sup>13,14,15</sup>, vibrations in solids<sup>16</sup> or electromagnetism<sup>17</sup>.

In the field of fluid mechanics, the presence of acoustics can affect the flow in a drastic manner in potentially unstable cases<sup>18,19,20</sup>. The numerical simulation of such flows in compressible codes is a major issue. Numerical boundary conditions must be treated with great caution to predict both the acoustic waves and the mean flow. Even though techniques have been developed to predict the mean flow in steady compressible codes (when acoustics are suppressed by numerical or physical viscosity) or to control the acoustic waves in linearized codes (where the mean flow is imposed), no method can handle both the mean flow and the acoustic waves in a perfect way: boundary conditions which allow a perfect control of the mean flow are generally reflecting acoustic waves while purely non-reflecting conditions used for example for linearized simulations will allow mean flow values to drift.

One example where such issues are critical is the prediction of combustion instabilities in reacting flows<sup>20,21,22,23,24</sup>. Many flames exhibit strong combustion instabilities when they are placed in a channel. These oscillations are due to a coupling between the flame and the channel acoustics (Fig.1-a). Acoustic waves are reflected in inlets and outlets and feedback in the domain where they can couple with the hydrodynamics and the unsteady heat release. A convenient method to characterize these instabilities is to study the forced response of the flame in the channel while “disconnecting” the coupling with the acoustics of the channel. This can be done experimentally by changing the channel geometry upstream or downstream of the burner. Numerically, the same result can be achieved by diminishing the acoustic feedback of the channel to the burner, i.e. by using non-reflecting boundary conditions on inlets and outlets (Fig. 1-b): this allows outgoing waves to leave the domain but cancels the amplitude of waves entering the domain, thereby diminishing the possible effects of coupling mechanisms. In certain cases, making only the outlet non-reflecting (Fig. 1-c) may be sufficient to stabilise the flow, as tested in section 5. There is no general rule indicating whether making boundaries non-reflecting in a given configuration will indeed be sufficient to damp the instability.

The decomposition of the Euler equations into characteristic waves is widely used to derive non-reflecting boundary conditions. A specific point which is common to all characteristic techniques is to prescribe the amplitude of the incoming waves<sup>3,13,14,5</sup>. The natural choice for non-reflecting bound-

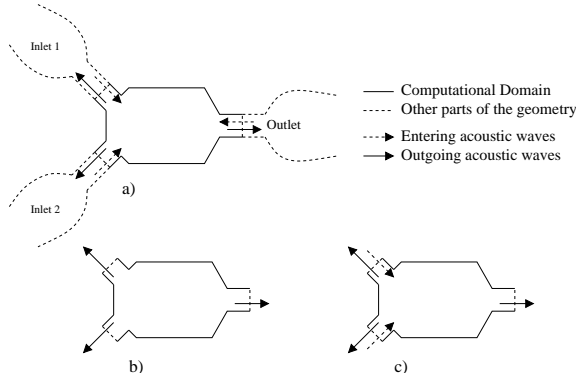


Figure 1: Waves entering and leaving the computational domain.

aries is to set this amplitude to zero. This method is well founded to control the acoustic field (when acoustic waves reach the boundary at normal incidence) but not the mean flow: different authors<sup>25,2</sup> indicate that this choice may lead to ill-posed problems. Indeed, setting for example a zero amplitude for the incoming wave ( $\mathcal{L}_1$ ) at a subsonic outlet (Fig. 2) may not allow the flow to keep a constant mean pressure. In the “real” world, the mean pressure is imposed by the state at infinity, downstream of the burner where the pressure is  $P_\infty$  and this information is fed back into the domain through  $\mathcal{L}_1$ : setting this value to zero is usually not a good choice, because the information on  $P_\infty$  is simply ignored by the code leading to possible drifts on the mean pressure. This problem is well known and various solutions have been proposed. One of them is to provide a value for  $\mathcal{L}_1$  either using an analytical solution in region 2, or solving a linear problem between the outlet section S and infinity (see recent review edited by Tourrette and Halpern<sup>26</sup>). Such solutions can only be used in certain academic cases for which an analytical solution may be derived between the outlet of the computational domain and the “infinity” condition<sup>16</sup>. More practical (but less accurate) solutions have been proposed. The simplest one (Linear Relaxation Method: LRM) is to set the amplitude of  $\mathcal{L}_1$  as proportional to the static pressure difference<sup>25,2</sup>:  $\mathcal{L}_1 = K(P - P_\infty)$  where  $P$  is the predicted pressure at the outlet section S,  $P_\infty$  is the far field pressure and  $K$  has the dimension of a frequency. “Appropriate” values of  $K$  are expected to provide a quasi non-reflecting boundary condition while avoiding pressure drifts: if  $P$  drifts away from  $P_\infty$ ,  $\mathcal{L}_1$  acts as a spring force to relax  $P$  towards  $P_\infty$ <sup>27</sup>.

Even though this relaxation approach is used today in multiple studies<sup>28</sup>, two questions arise:

- Are there optimal choices for  $K$ ?

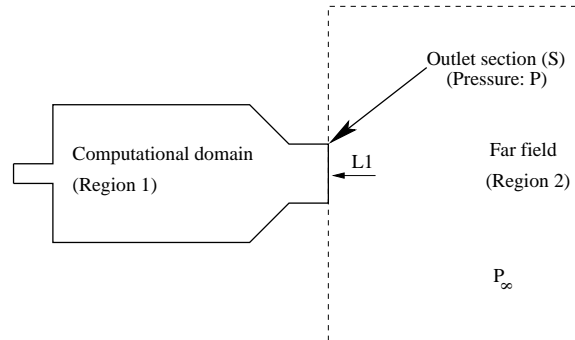


Figure 2: Influence of far field conditions on the amplitude of the waves entering the computational domain.

- What is the effect of this relaxation on the global acoustic behaviour of the boundary?

Obviously, low levels of  $K$  may be inefficient in terms of controlling the mean pressure. Inversely, high levels of  $K$  ensure that  $P$  remains very close to  $P_\infty$  and then make the boundary partially or fully reflecting. Therefore, a direct link exists between the magnitude of  $K$  and the reflection coefficient  $R$  of the boundary. Actually,  $K$  controls not only the magnitude of  $R$ , but also its phase. Choosing  $K$  without care may lead to numerical results in which the outlet boundary condition introduces important biases in terms of acoustic behaviour of the flow.

The objectives of this paper are:

- to derive a simple analytical solution relating the magnitude of the relaxation coefficient  $K$  and the complex reflection coefficient  $R$  of a boundary condition modeled with LRM (Section 3),
- to verify this relation using corresponding numerical simulations in which the outlet of a simple tube is submitted to a harmonic propagating wave (Section 4),
- to demonstrate the effect of non-reflecting boundary condition using LRM on the global resonance of a given duct: here a simple case with fixed inlet velocity and non-reflecting LRM outlet is studied both analytically and numerically (Section 5),
- finally, to propose a method to scale the  $K$  coefficient in practical computations (Section 6).

It will be shown that the values of  $K$  control the damping rate of the modes, but may also change significantly the eigenvalues. In other words, a non optimal choice of  $K$  may lead to erroneous resonant frequencies.

## 2 Waves amplitudes

The following developments are based on the method derived by Poinso and Lele<sup>2</sup> called NSCBC (Navier-Stokes Characteristic Boundary Conditions). In all characteristic approaches, the main issue is the determination of the amplitudes of waves entering the computational domain. In the NSCBC method, the determination is based on the assumption that the amplitudes can be obtained as if the flow was laminar, one dimensional and inviscid (LODI). Note that for 1D non-viscous flows, the NSCBC method is equivalent<sup>26,29</sup> to many other boundary treatments<sup>3,13,14,30</sup> so that the results presented in section 3 apply to all charecteristic techniques using LRM.

LODI equations (1, 2, 3, 4, and 5) link the waves amplitudes ( $\mathcal{L}_i$ ) and the temporal evolution of primitive Navier-Stokes variables ( $\rho, u, v, w, P$ ). The waves amplitudes  $\mathcal{L}_1, \mathcal{L}_2, \mathcal{L}_3, \mathcal{L}_4, \mathcal{L}_5$  correspond respectively to the left travelling acoustic wave (speed  $u - c$ ), the entropy wave (speed  $u$ ), the first vorticity wave (speed  $u$ ), the second vorticity wave (speed  $u$ ), and the right travelling acoustic wave (speed  $u + c$ ). Their expression is obtained through characteristic analysis<sup>2,27</sup>:

$$\frac{\partial \rho}{\partial t} + \frac{1}{c^2} \left[ \mathcal{L}_2 + \frac{1}{2}(\mathcal{L}_5 + \mathcal{L}_1) \right] = 0 \quad (1)$$

$$\frac{\partial u}{\partial t} + \frac{1}{2\rho c}(\mathcal{L}_5 - \mathcal{L}_1) = 0 \quad (2)$$

$$\frac{\partial v}{\partial t} + \mathcal{L}_3 = 0 \quad (3)$$

$$\frac{\partial w}{\partial t} + \mathcal{L}_4 = 0 \quad (4)$$

$$\frac{\partial P}{\partial t} + \frac{1}{2}(\mathcal{L}_5 + \mathcal{L}_1) = 0 \quad (5)$$

where the waves amplitudes  $\mathcal{L}_1, \dots, \mathcal{L}_5$  are defined by:

$$\mathcal{L}_1 = (u_1 - c) \left( \frac{\partial P}{\partial x_1} - \rho c \frac{\partial u_1}{\partial x_1} \right) \quad (6)$$

$$\mathcal{L}_2 = u_1 \left( c^2 \frac{\partial \rho}{\partial x_1} - \frac{\partial P}{\partial x_1} \right) \quad (7)$$

$$\mathcal{L}_3 = u_1 \frac{\partial u_2}{\partial x_1} \quad (8)$$

$$\mathcal{L}_4 = u_1 \frac{\partial u_3}{\partial x_1} \quad (9)$$

$$\mathcal{L}_5 = (u_1 + c) \left( \frac{\partial P}{\partial x_1} + \rho c \frac{\partial u_1}{\partial x_1} \right) \quad (10)$$

Eq. 1 to 5 provide a simple method to choose the incoming waves amplitudes to be imposed at a boundary. For example, from Eq. 2, a fixed velocity inlet condition will require the incoming wave amplitude  $\mathcal{L}_5$  to be equal to the outgoing wave  $\mathcal{L}_1$ . Fixing a constant pressure at an outlet will be achieved (from Eq. 5) by setting  $\mathcal{L}_1 = -\mathcal{L}_5$ . A more critical situation arises to mimic non-reflecting conditions: this would require to set the incoming waves to zero. As indicated earlier, such a "perfectly" non-reflecting condition is not adequate because it may lead to a drift of the mean flow quantities. The next section illustrates the behaviour of a duct outlet for which a non-reflecting condition is sought.

### 3 The reflection coefficient of a LRM boundary condition

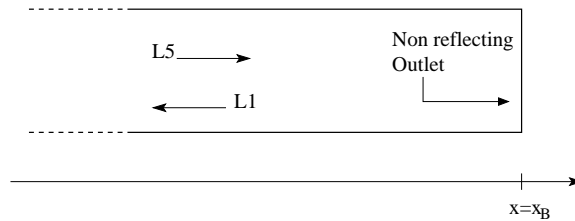


Figure 3: 1D harmonic wave impacting on the outlet boundary of a tube

Let us consider the propagation of one-dimensional acoustic waves in a semi-infinite tube of constant cross section (Fig. 3). The tube is infinite in the  $x < 0$  direction and ends at  $x = x_B$  in the other direction where a non-reflecting boundary condition must be implemented. An harmonic wave

propagating in increasing  $x$  direction is imposed. The expression<sup>1</sup> of this complex wave at  $x = x_B$  is taken as:

$$\mathcal{L}_5 = 2\rho c U_0 i \omega e^{-i\omega t} \quad (11)$$

The objective of the condition at  $x = x_B$  is to be non-reflecting. In practice, to avoid a drift of the mean pressure, the incoming wave amplitude  $\mathcal{L}_1$  is not set to zero but to:

$$\mathcal{L}_1 = K(P - P_\infty) \quad (12)$$

Eq. 11 and 12, together with LODI relations 2 and 5 lead to the system of equations:

$$\begin{cases} \frac{\partial u}{\partial t} + \frac{1}{2\rho c}(2\rho c U_0 i \omega e^{-i\omega t} - K(P - P_\infty)) = 0 \\ \frac{\partial P}{\partial t} + \frac{1}{2}(2\rho c U_0 i \omega e^{-i\omega t} + K(P - P_\infty)) = 0 \end{cases} \quad (13)$$

The second equation of system 13 only involves  $P$  and can easily be solved<sup>2</sup>. The solution for  $P$  including transient regime is:

$$P(t) = P_\infty + A_0 e^{-\frac{Kt}{2}} - \frac{\rho c U_0 i \omega}{\frac{K}{2} - i\omega} e^{-i\omega t} \quad (14)$$

The transient term  $A_0 e^{-\frac{Kt}{2}}$  of Eq. 14 ( $A_0$  being a constant fixed by initial conditions) always vanishes with time since  $K > 0$ . In further developments, it will be assumed that a steady state has been reached and this term will be omitted.

Eq. 14 (without transient part) and Eq. 12 allow to reconstruct the incoming wave  $\mathcal{L}_1$  and then, the complex reflection coefficient of the boundary. The analytical value of the reflection coefficient  $R$  is:

$$R_{out} = \frac{\mathcal{L}_1}{\mathcal{L}_5} = -\frac{1}{1 - i\frac{2\omega}{K}} \quad (15)$$

The magnitude ( $\|R\|$ ) and phase ( $\phi$ ) of a non-reflecting outlet modeled with LRM are derived from Eq. 15 (The asymptotic behaviour of  $\|R\|$  and  $\phi$  is summarised in table 1):

$$\|R\| = \frac{1}{\sqrt{1 + (\frac{2\omega}{K})^2}} \quad (16)$$

---

<sup>1</sup>This wave amplitude is chosen so that in the absence of reflected wave, the inlet velocity signal would be  $u(t) = U_0 e^{-i\omega t}$ . Note that the phase is set to zero at  $x = x_B$  to simplify the algebra. It has no influence on the result.

<sup>2</sup>This system was derived at the outlet boundary, consequently, coordinates are fixed and both  $u$  and  $P$  are functions of time only.

$$\phi = -\pi - \arctan\left(\frac{2\omega}{K}\right) \quad (17)$$

Pulsation	$\ R\ $	$\phi$
$\omega = 0$	1	$-\pi$
$\omega = \frac{K}{2}$	$\frac{1}{\sqrt{2}}$	$-\pi - \frac{\pi}{4}$
$\omega = \infty$	0	$-\frac{3\pi}{2}$

Table 1: Asymptotic behaviour of a non-reflecting outlet with LRM.

As expected, for a given pulsation  $\omega$ ,  $\|R\|$  goes to 0 when  $K$  is small, showing that the boundary condition is indeed non-reflecting ( $\|R\| \simeq 0$ ) when  $K$  is limited to small values. However, large values of  $K$  destroy the "non-reflecting" character of the boundary condition: when  $K$  goes to infinity,  $\|R\|$  goes to 1 making the boundary fully reflecting. Actually, as shown by Eq. 16 the control parameter for  $\|R\|$  is  $2\omega/K$ , so that one can define a cut-off pulsation  $\omega_c = K/2$ . For a fixed value of  $K$  (which is the case in any computation), all frequencies will not be reflected with the same strength. High frequencies will easily leave the computational domain ( $R \rightarrow 0$ ) whereas very low frequencies will be strongly reflected ( $R \rightarrow 1$ ). In practice, a cut-off frequency  $f_c$  separates waves that will be reflected ( $f < f_c$ ) from the ones that will leave the domain ( $f > f_c$ ).  $f_c$  is defined from Eq. 15 by:

$$f_c = \frac{\omega_c}{2\pi} = \frac{K}{4\pi} \quad (18)$$

This definition imposes that  $R(f_c) = 1/\sqrt{2}$ . In terms of energy, this means that at the frequency  $f_c$  half of the acoustic energy is fed back into the computational domain.

Fig. 4 is a plot of Eq. 16 and 17. The cut-off frequency  $f_c$  is represented by the vertical line. Eq. 18 suggests that a proper interpretation of  $K$  is to view  $f_c = K/(4\pi)$  as a frequency below which the boundary condition will not let the waves leave the domain.

At constant  $K$ , the phase  $\phi$  of the reflected signal is that of a fixed pressure outlet for low values of  $\omega$ . But as shown in Fig. 4, when the frequency increases, the boundary treatment induces a delay that moves the phase from  $-\pi$  to  $-3\pi/2$ . This phase shift can induce dramatic changes in the acoustic properties of the domain as shown in section 5.

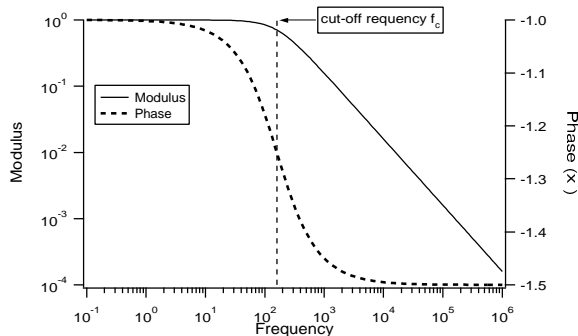


Figure 4: Modulus and phase of reflection coefficient versus frequency at  $K = 2000s^{-1}$ .

## 4 Numerical evaluation of the reflection coefficient

In this section, Eq. 15 is compared to numerical simulations. This is done by simply running a full Euler code on the configuration of Fig. 3 and using Eq. 12 at the outlet. The code AVBP<sup>3</sup> was used for this validation. AVBP is a 3D fully compressible Navier Stokes solver using characteristic boundary conditions<sup>2</sup>.

The outlet condition is non-reflecting (with LRM), as described in section 3, and the inlet is a non-reflecting pulsated inlet<sup>31</sup>. The numerical scheme is 2<sup>nd</sup> order in space, and uses a 3 step Runge-Kutta method (3<sup>rd</sup> order) for time integration. Calculation parameters are summarized in table 2.

Size of the domain $L$ (m)	0, 5
Number of cells	400
Mean inlet velocity ( $m.s^{-1}$ )	10
Sound speed $c$ ( $m.s^{-1}$ )	348
Forcing frequency $f$ (Hz)	500
Forcing amplitude ( $m.s^{-1}$ )	0.1

Table 2: Summary of numerical simulation parameters.

For technical reasons, it is more convenient to vary  $K$  at the outlet than to change the forcing frequency  $f$  at the inlet. Therefore, the following results present  $R(K)$  at fixed  $f$  instead of  $R(f)$  at fixed  $K$ . The reflection

<sup>3</sup>AVBP home page for detailed information: <http://www.cerfacs.fr/cfd/CFDWeb.html>

coefficient  $R$  is obtained in AVBP by  $R = \mathcal{L}_1/\mathcal{L}_5$ . The amplitudes  $\mathcal{L}_1$  and  $\mathcal{L}_5$  are measured at the outlet using Eq. 6 and 10 and one sided spatial derivatives.

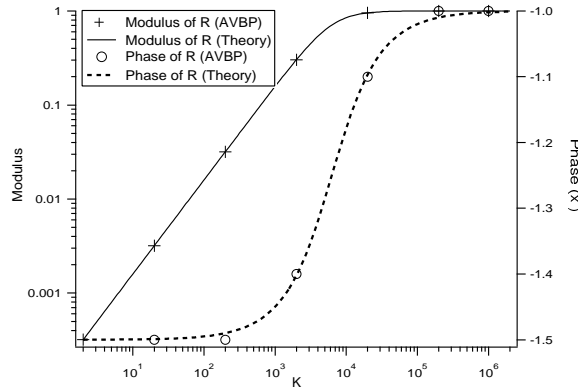


Figure 5: Comparison of numerical and theoretical reflection coefficient at a "partially reflecting" outlet.

The agreement between numerical simulations and the theory (Eq. 15) is extremely good (Fig. 5). Both modulus and phase of the reflection coefficient at the outlet are superimposed to the theoretical curves.

## 5 Computing a closed domain with non-reflecting boundary condition

### 5.1 Description of the configuration

The previous sections have shown that non-reflecting boundary conditions using LRM can have impedances which make them partially reflecting. This section shows the implications of these results for the computation of flows where one (or more) section is modeled using such non-reflecting conditions.

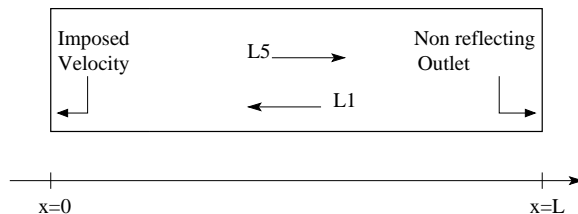


Figure 6: Configuration

Consider a simple duct filled with an homogeneous gas (in which the speed of sound  $c$  is constant) as represented in Fig. 6. The inlet speed is imposed:  $u(x = 0, t) = U_0$ . The steady flow solution is of course:  $u(x, t) = U_0$ . This system is acoustically defined by its reflection coefficients at the inlet and the outlet. Assuming that the duct inlet is the phase reference, one can write the relations between the amplitude of the acoustic waves in the duct, and the reflection coefficients:

$$\begin{cases} R_{in} &= \frac{\mathcal{L}_5}{\mathcal{L}_1} \\ R_{out} &= \frac{\mathcal{L}_1 e^{-i\omega \frac{L}{c}}}{\mathcal{L}_5 e^{i\omega \frac{L}{c}}} \end{cases} \quad (19)$$

which can be written as:

$$R_{in} R_{out} e^{i\omega \frac{2L}{c}} - 1 = 0 \quad (20)$$

Calculating the eigen-frequencies of this duct consists in giving the values of  $\omega$  which are solutions of Eq. 20.

## 5.2 Analytical solutions

For this test, the inlet corresponds to fixed velocity conditions which implies  $R_{in} = 1$ . The outlet is modeled using a non-reflecting condition with LRM. Therefore Eq. 15 shows that the effective impedance of this outlet is  $R_{out} = -1/(1 - i(2\omega/K))$ . In this case, Eq. 20 degenerates to:

$$e^{i\omega \frac{2L}{c}} + \left(1 - i\frac{2\omega}{K}\right) = 0 \quad (21)$$

The values of  $\omega$  that satisfy Eq. 21 are complex. The real part of  $\omega$  ( $\omega_r = \Re(\omega) = 2\pi f_r$ ) is the eigen-pulsation, and the imaginary part ( $\omega_i = \Im(\omega) = 2\pi f_i$ ) is the damping (or amplification) rate. The temporal evolutions of pressure and velocity at an eigen-frequency are proportional to  $e^{-i\omega t} = e^{-i\omega_r t} e^{\omega_i t}$  (in the linear regime):

- If  $\omega_i > 0$ , the mode is amplified:  $\omega_r$  is an unstable pulsation,
- if  $\omega_i < 0$ , the mode is damped:  $\omega_r$  is a stable pulsation.

Fig. 7 is a plot of the eigen-frequencies of Eq. 21 versus  $K$ . At very high values of  $K$ , the system responds as if the pressure were fixed at the outlet<sup>4</sup>, and the eigen-frequencies (Eq. 22) correspond directly to the 1/4

---

<sup>4</sup>Combining Eq. 11, 12 and 14, one can show that  $\mathcal{L}_5 + \mathcal{L}_1$  goes to zero when  $K$  goes to infinity.

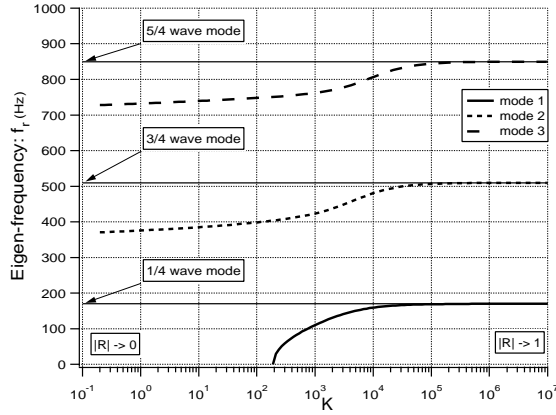


Figure 7: Eigen-frequencies of the first 3 modes versus  $K$  for the duct of Fig. 6.

wave ( $n = 0$ ), 3/4 wave ( $n = 1$ ),... modes of a duct with fixed inlet velocity and outlet pressure (represented by horizontal lines in Fig. 7): the boundary is fully reflecting.

$$f_n = (2n + 1) \frac{c}{4L} \quad (22)$$

When  $K$  decreases, the eigen-frequencies of the duct also decrease due to the phase shift induced by the boundary treatment shown by Eq. 17. At very low  $K$  values, the 1/4 wave mode even disappears.

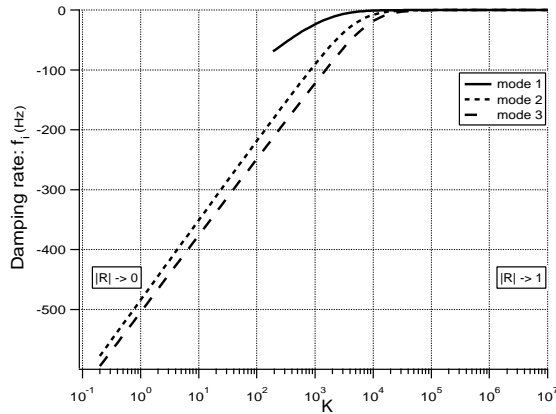


Figure 8: Imaginary part of the first 3 modes versus  $K$  for the duct of Fig. 6.

At very high values of  $K$ , the imaginary part  $f_i$  of all eigen-frequencies is zero (Fig. 8), indicating that they are not damped. This is consistent with

the fact that there is no source term in the duct and boundary conditions are acoustically closed (no fluctuation of  $P$  or  $u$  allowed). Obviously, at such large  $K$  values, the outlet boundary condition fails to evacuate acoustic waves. For lower values of  $K$ , the modulus of  $R_{out}$  is lower than 1 and thus all modes are damped ( $\Im(\omega) < 0$ ).

Fig. 7 and 8 show that the value of  $K$  must remain small to provide damped modes but also that the modes which appear are not physical: their frequencies are not the eigen-frequencies of the duct.

## 6 A scaling strategy for the relaxation coefficient $K$

As shown in the previous sections, the value of  $K$  has a drastic influence on the results of a numerical simulation. This has already been pointed out by different authors, either for steady<sup>25</sup>, or unsteady<sup>2</sup> calculations. The main problem for several authors is to know how to choose  $K$  in practical cases. Rudy and Strikwerda<sup>25</sup> suggested the following scaling of  $K$  for optimal convergence of steady calculations:

$$K = \sigma(1 - \mathcal{M}^2) \frac{c}{L} \quad (23)$$

where  $\mathcal{M}$  is the Mach number of the mean flow,  $c$  the sound speed and  $L$  the domain size.

Numerical simulations<sup>25,2,27</sup> showed that an optimum is reached for  $\sigma_{Num}^{optim} = 0.58$  while the theory of Rudy and Strikwerda<sup>25</sup> suggested an optimum value of  $\sigma_{RS}^{optim} = 0.27$ .

The present work gives a new interpretation of  $K$  which is now linked to the cut-off frequency of the boundary by Eq. 18. Thus "good" values of  $K$  are those which allow all duct acoustic modes to leave the domain. It was shown in section 3 that frequencies lower than  $f_c = K/(4\pi)$  are reflected, and frequencies higher than  $f_c$  leave the computational domain. It is then relevant to choose  $K$  so that  $f_c$  is lower than all acoustic frequencies expected in the computational domain.

As an example, this strategy is now applied to the duct of section 5. Since velocity is imposed at the inlet, and pressure at the outlet, the lowest acoustic frequency expected is that of a quarter-wave mode. At a given Mach number  $\mathcal{M}$ , the quarter-wave mode frequency is:

$$f_0 = (1 - \mathcal{M}^2) \frac{c}{4L} \quad (24)$$

From Eq. 18 and 24, the highest value of  $K$  for this calculation, which will significantly damp the 1/4 wave mode (as well as other higher order modes) is:

$$K^{max} = \pi(1 - \mathcal{M}^2)\frac{c}{L} \quad (25)$$

This scaling of  $K$  is very similar to the theory of Rudy and Strikwerda<sup>25</sup> given in Eq. 23 but with a  $\sigma$  coefficient of  $\pi$  instead of 0.58. This approach suggests that the highest admissible value of  $\sigma$  to prevent acoustic feed back is:

$$\sigma^{max} = \pi \quad (26)$$

On the other hand,  $K$  (or  $\sigma$ ) has to be chosen large enough to prevent a drift in the mean values (pressure, mass flow...). The minimum admissible value  $\sigma_{min}$  is not fixed by acoustics. It strongly depends on the computation parameters (Reynolds number, 3D effects such as swirl, geometry...). Other tests (not reported here) suggest that choosing  $\sigma$  lower than 0.1 often increases convergence times and sometimes does not allow mass fluxes and pressure to reach a steady state.

Fig. 9 offers a simple summary of these findings.

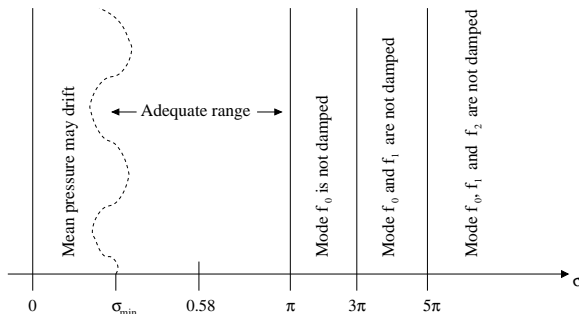


Figure 9: Summary of the influence of  $\sigma$  on the acoustics and mean flow quantities.

## 7 Numerical Computations

Section 5.2 has provided a theoretical stability analysis of the duct of Fig. 6. In the present section, these results are tested numerically in AVBP. The duct inlet is a fully reflecting characteristic inlet with imposed velocity<sup>5</sup>. A

<sup>5</sup>Achieved through LODI relation 2 by imposing  $\mathcal{L}_5 = \mathcal{L}_1$

non-reflecting outlet with LRM is applied at the outlet: the value of  $\sigma$  is varied to illustrate the results of sections 5 and 6. A gaussian perturbation is superimposed to the initial pressure field to excite all acoustic modes.

Two values for  $\sigma$  are investigated to illustrate the influence on both the damping of acoustics, and the shift of the eigen-frequencies of the duct.

## 7.1 Case 1: $\sigma = 10 * \pi$

In this section, the relaxation factor at the outlet  $\sigma$  is fixed to  $\sigma = 10 * \pi$  which is too high to evacuate the first eigen-modes of the duct. The pressure

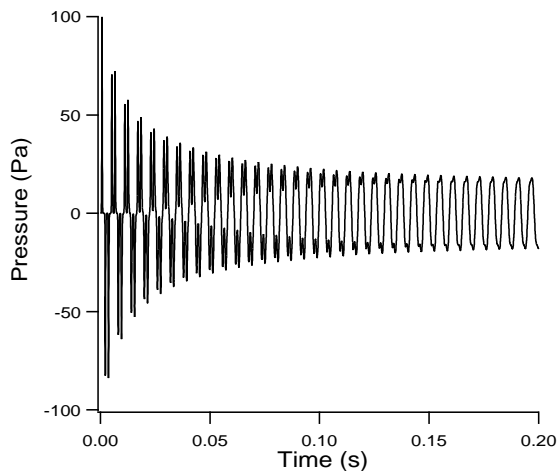


Figure 10: Time evolution of pressure perturbation at the inlet ( $\sigma = 10 * \pi$ ).

perturbations, recorded at the inlet show an exponential decay (Fig. 10) before  $t = 0.1s$  corresponding to the evacuation of high frequency modes. The signal then remains almost constant since low frequency modes are reflected by the condition at the outlet.

Fig. 11 is the Fourier transform of the inlet pressure signal. The spectrum is compared to the expected eigen-frequencies analytically derived in section 5. The first three modes predicted by Eq. 21 and displayed in Fig. 11 remain in the computational domain as suggested from Fig. 9 for  $\sigma = 10\pi$ . Moreover, the frequencies of these modes are not the true eigen-frequencies as predicted by Eq. 22 which gives the eigen-frequencies of an acoustically closed duct (imposed velocity at the inlet and imposed pressure at the outlet). This confirms the biasing effects induced by the outlet condition when large values of  $\sigma$  are used:

- the outlet is strongly reflecting so that certain modes are not damped and

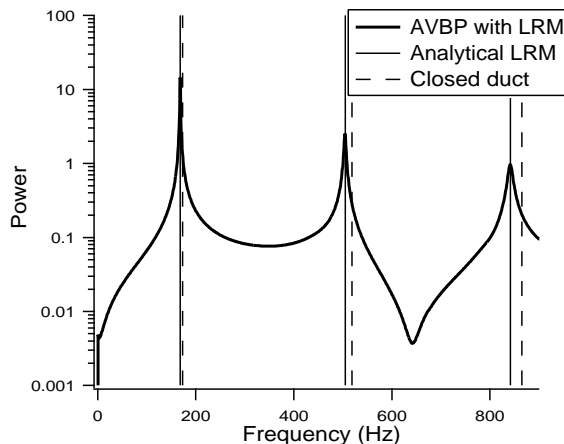


Figure 11: Spectrum of pressure signal ( $\sigma = 10 * \pi$ ) compared to analytical values of section 5 and Eq. 22.

- the frequencies of the modes differ from the true eigen-frequencies of the duct.

Obviously, this would not be a good choice for  $\sigma$  for practical computations.

The agreement between numerical and analytical results is good, the shift between the eigen-frequencies of the closed duct, and the duct with LRM is correctly predicted.

## 7.2 Case 2: $\sigma = \pi$

In this section,  $\sigma = \pi$ , which is the highest value that enables the evacuation of all acoustic modes of the duct.

Fig. 12 shows the exponential decay of the pressure perturbations. At  $t = 0.1s$  all acoustic modes have vanished. Note that there is no source term in the domain and that the simulation is quite long compared to  $f_c$  (35 cycles) so that even a reflection coefficient slightly lower than 1 (the definition of the cut-off frequency  $f_c$  is so that  $R = 1/\sqrt{2}$ .) enables to attenuate the mode.

Fig. 13 is the Fourier transform of the pressure signal of Fig. 12 between  $t = 0$  and  $t = 0.05s$ . The spectrum is compared to the expected eigen-frequencies analytically derived in section 5, and to the true eigen-frequencies of the duct given by Eq. 22. The spectrum is not very sharp due to the exponential decay of the signal and yet, the agreement is fairly good. Again, the eigen-frequencies of the duct are significantly shifted compared to an acoustically closed duct.

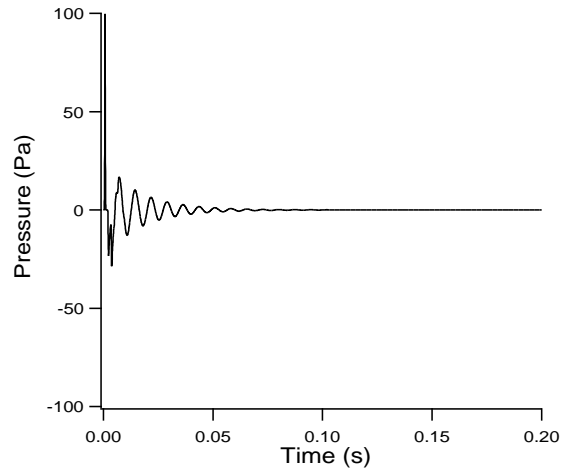


Figure 12: Time evolution of pressure perturbation at the inlet ( $\sigma = \pi$ ).

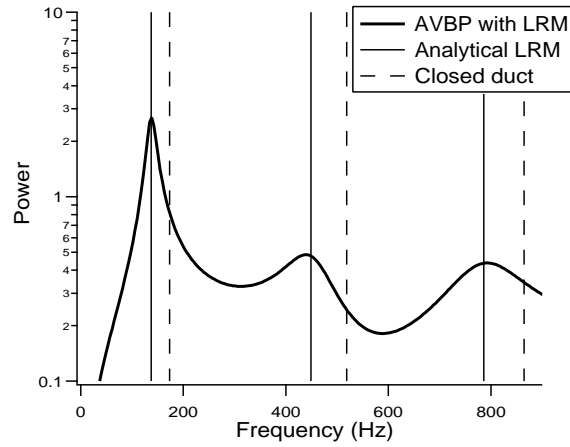


Figure 13: Spectrum of pressure signal ( $\sigma = \pi$ ) compared to analytical values of section 5 and Eq. 22.

## 8 Conclusion

A simple acoustic theory was proposed to characterize the actual reflection coefficient of numerical "non-reflecting" boundary condition using LRM (Linear Relaxation Method) as proposed by Rudy and Strikwerda<sup>25</sup> or Poinso and Lele<sup>2</sup>. It has been shown that large values of the relaxation coefficient  $K$  used in these methods to link the ingoing wave amplitude  $\mathcal{L}_1$  to the pressure difference  $(P - P_\infty)$ , make the boundary condition fully reflecting and that  $K$  can be linked to a cut-off frequency  $f_c$  by  $K = 4\pi f_c$ . At a given value of  $K$ , all modes such that  $f < f_c$  are not damped. A proper strategy to minimize acoustics coupling is to choose  $K$  so that  $f_c$  is lower than the first duct acoustic mode. In the case of a 1D duct with imposed velocity inlet, this is obtained by writing  $K = \sigma(1 - \mathcal{M})(c/L)$  and choosing  $0.2 < \sigma < \pi$ . For more complex cases (3D, complex geometries, combustion...), an extension of this strategy is to solve the general equation of acoustics in the domain to find its eigen-frequencies  $f_i$ . The maximum value of  $\sigma$  is then given by choosing  $f_c = \min(f_i)$ .

## 9 References

<sup>1</sup>Engquist, B. & Majda, A., "Absorbing boundary conditions for the numerical simulation of waves," *Math. Comput.*, Vol. 31, 139, 1977, pp. 629-651.

<sup>2</sup>Poinso, T. & Lele, S., "Boundary conditions for direct simulations of compressible viscous flows," *J. Comput. Phys.*, Vol. 101, 1, 1992, pp. 104-129.

<sup>3</sup>Hirsch, C., *Numerical Computation of internal and external flows*. John Wiley, 1988.

<sup>4</sup>Hagstrom, T. & Hariharan, S. I., "Accurate Boundary Conditions for Exterior Problems in Gas Dynamic," *Mathematics of Computation*, Vol. 51, 1988, pp. 581-597.

<sup>5</sup>Tourrette, L., "Artificial Boundary conditions for the Linearized Compressible Navier-Stokes Equations," *J. Comput. Phys.*, Vol. 137, 1997, pp. 1-37.

<sup>6</sup>Hayder, M. E. & Turkel, E., "Nonreflecting Boundary Conditions for Jet Flow Computations," *AIAA J.*, Vol. 33, 1995, pp. 2264-2270.

<sup>7</sup>Tsynkov, S. V., "Numerical Solution of Problems on Unbounded Domains. A Review," *Applied Numerical Mathematics: Transactions of IMACS*, Vol. 27, 1998, pp. 465-532.

<sup>8</sup>Vasilyev, O. V. & Bowman, C., "Second-generation wavelet collocation method for the solution of partial differential equations," *J. Comput. Phys.*,

Vol. 165, 2, 2000, pp. 660-693.

<sup>9</sup>Kim, J. W. & Lee, D. J., "Generalized Characteristic Boundary Conditions for Computational Aeroacoustics," *AIAA J.*, Vol. 38, 2000, pp. 2040-2049.

<sup>10</sup>Colonius, T., Lele, S. & Moin, P., "Boundary conditions for direct computation of aerodynamic sound generation," *AIAA Journal*, Vol. 31, 9, 1993, pp. 1574-1582.

<sup>11</sup>Rowley, C. W. & Colonius, T., "Discretely Nonreflecting Boundary Conditions for Linear Hyperbolic Systems," *J. Comput. Phys.*, Vol. 157, 2000, pp. 500-538.

<sup>12</sup>Freund, J. B., "Proposed Inflow/Outflow Boundary Condition for Direct Computation of Aerodynamic Sound," *AIAA J.*, Vol. 35, 1997, pp. 740-742.

<sup>13</sup>Thompson, K. W., "Time dependent boundary conditions for hyperbolic systems," *J. Comput. Phys.*, Vol. 68, 1987, pp. 1-24.

<sup>14</sup>Thompson, K. W., "Time dependent boundary conditions for hyperbolic systems," *J. Comput. Phys.*, Vol. 89, 1990, pp. 439-461.

<sup>15</sup>Grappin, R., Lorat, J. & Buttighoffer, A., "Alfvén Wave Propagation in the High Sonar Corona," *Astron. Astrophys.*, Vol. 362, 2000, pp. 342-358.

<sup>16</sup>Barry, A., Bielak, J. & MacCamy, R. C., "On Absorbing Boundary Conditions for Wave Propagation," *J. Comput. Phys.*, Vol. 79, 1988, pp. 449-468.

<sup>17</sup>Mur, G., "Absorbing boundary conditions for the finite-difference of the time-domain electromagnetic-field equations," *IEE trans. on Electromagnetic compatibility*, Vol. 23, 1981, pp. 377-382.

<sup>18</sup>Ho, C. M. & Huerre, P., "Perturbed free shear layers," *J. Fluid Mech.*, Vol. 16, 1984, pp. 365.

<sup>19</sup>Lucas, L. & Rockwell, D., "Self-excited jet: upstream modulation and multiple frequencies," *J. Fluid Mech.*, Vol. 147, 1984, pp. 333-352.

<sup>20</sup>Crighton, D. G., Dowling, A., Heckl, M., Leppington, F. & Williams, J., *Modern methods in analytical acoustics*. Springer Verlag, 1992.

<sup>21</sup>Yang, V. & Culick, F. E. C., "Analysis of low-frequency combustion instabilities in a laboratory ramjet combustor," *Combust. Sci. Tech.*, Vol. 45, 1986, pp. 1-25.

<sup>22</sup>Poinsot, T., Trouvé, A., Veynante, D., Candel, S. & Esposito, E., "Vortex driven acoustically coupled combustion instabilities," *J. Fluid Mech.*, Vol. 177, 1987, pp. 265-292.

<sup>23</sup>McManus, K., Poinsot, T. & Candel, S., "A review of active control of combustion instabilities," *Prog. Energy Comb. Sci.*, Vol. 19, 1993, pp. 1-29.

<sup>24</sup>Angelberger, C., Egolfopoulos, F. & Veynante, D., "Large Eddy Simulations of chemical and acoustic effects on combustion instabilities," *Flow Turb. and Combustion*, Vol. 65, 2, 2000, pp. 205-222.

<sup>25</sup>Rudy, D. H. & Strikwerda, J. C., "A non-reflecting outflow boundary condition for subsonic Navier Stokes calculations," *J. Comput. Phys.*, Vol. 36, 1980, pp. 55-70.

<sup>26</sup>Tourrette, L. & Halpern, L., *Absorbing Boundaries and Layers, Domain Decomposition Methods. Applications to Large Scale Computation.* Nova Science, 2001.

<sup>27</sup>Poinsot, T. & Veynante, D., *Theoretical and numerical combustion.* R.T. Edwards, 2001.

<sup>28</sup>Wall, C., Pierce, C. D. & Moin, P., "A Semi-implicit Method for Resolution of Acoustic Waves in Low Mach Number Flows," *J. Comput. Phys.*, Vol. 181, 2002, pp. 545-563.

<sup>29</sup>Nicoud, F., "Defining wave amplitude in characteristic boundary conditions," *J. Comput. Phys.*, Vol. 149, 2, 1998, pp. 418-422.

<sup>30</sup>Giles, M., "Non-reflecting boundary conditions for Euler equation calculations," *AIAA Journal*, Vol. 28, 12, 1990, pp. 2050-2058.

<sup>31</sup>Kaufmann, A., Nicoud, F. & Poinsot, T., "Flow Forcing Techniques for Numerical Simulation of Combustion Instabilities," *Combust. Flame*, Vol. 131, 2002, pp. 371-385.